### **OPEN ACCESS**



# Compact Steep Spectrum Radio Sources with Enhanced Star Formation Are Smaller Than 10 kpc

Yjan A. Gordon <sup>1</sup>, Christopher P. O'Dea <sup>2</sup>, Stefi A. Baum <sup>2</sup>, Keith Bechtol <sup>1</sup>, Chetna Duggal <sup>2</sup>, and Peter S. Ferguson <sup>1</sup>, Department of Physics, University of Wisconsin-Madison, 1150 University Ave., Madison, WI 53706, USA; yjan.gordon@wisc.edu <sup>2</sup> Department of Physics and Astronomy, University of Manitoba, Winnipeg, MB R3T 2N2, Canada Received 2023 February 22; revised 2023 April 12; accepted 2023 April 20; published 2023 May 2

#### **Abstract**

Compact steep spectrum (CSS) radio sources are active galactic nuclei (AGN) that have radio jets propagating only on galactic scales, defined as having projected linear size (LS) of up to 20 kpc. CSS sources are generally hosted by massive early-type galaxies with little ongoing star formation; however, a small fraction are known to have enhanced star formation. Using archival data from the Faint Images of the Radio Sky at Twenty cm survey, the Very Large Array Sky Survey, and the Sloan Digital Sky Survey, we identify a volume-limited sample of 166 CSS sources at z < 0.2 with  $L_{1.4 \text{ GHz}} > 10^{24}$  W Hz<sup>-1</sup>. Comparing the star formation rates and linear sizes of these CSS sources, we find that the  $\approx 14\%$  of CSS sources with specific star formation rates above 0.01 Gyr<sup>-1</sup> all have LS < 10 kpc. We discuss the possible mechanisms driving this result, concluding that it is likely the excess star formation in these sources occurred in multiple bursts and ceased prior to the AGN jet being triggered.

*Unified Astronomy Thesaurus concepts:* AGN host galaxies (2017); Active galactic nuclei (16); Extragalactic radio sources (508); Radio galaxies (1343); Star formation (1569)

#### 1. Introduction

Active galactic nuclei (AGN) are the phenomenon whereby matter is accreting onto the central supermassive black hole of their host galaxies (Salpeter 1964). A small fraction of AGN produce particle jets that result in radio emission via mechanisms such as synchrotron radiation and inverse Compton scattering (Padovani 2017; Blandford et al. 2019). The jets produced by these radio-loud AGN (RLAGN) can sometimes propagate well beyond the host galaxy, giving rise to large scale double-lobed structures such as Fanaroff and Riley class I and II radio galaxies (FRIs and FRIIs; Fanaroff & Riley 1974) that can span hundreds of kiloparsecs or more (e.g., Willis et al. 1974; Ishwara-Chandra & Saikia 1999; Dabhade et al. 2017). In contrast to FRIs and FRIIs are compact RLAGN that have radio emission on scales similar to or smaller than the host galaxy.

Compact steep spectrum (CSS) radio sources have radio extents smaller than ~20 kpc and radio spectral indices of  $\alpha < -0.5$ , where spectral index,  $\alpha$ , is related to flux density, S, and frequency,  $\nu$ , by  $S \propto \nu^{\alpha}$  (Fanti et al. 1990; O'Dea 1998; O'Dea & Saikia 2021). It is thought that at least some CSS sources are young AGN that will evolve into larger radio morphologies (Fanti et al. 1995; O'Dea 1998; An & Baan 2012; O'Dea & Saikia 2021). This hypothesis is based on very long baseline interferometry (VLBI) observations of powerful CSS sources that show double-lobed radio morphologies analogous to FRIs and FRIIs but on a much smaller scale (Spencer et al. 1991; Dallacasa et al. 1995), and jet proper motions indicative of a short travel time from the central engine (Owsianik & Conway 1998; Polatidis & Conway 2003; An et al. 2012). The young AGN scenario is further supported by CSS sources having host galaxies similar those of larger radio galaxies.

Original content from this work may be used under the terms of the Creative Commons Attribution 4.0 licence. Any further distribution of this work must maintain attribution to the author(s) and the title of the work, journal citation and DOI.

An alternative to the young AGN scenario, is that the radio jets in CSS sources are unable to travel as easily through the interstellar medium (ISM), a phenomenon known as "frustration" (van Breugel et al. 1984; Wilkinson et al. 1984; O'Dea et al. 1991). Frustration can occur either as a result of intrinsically weak jet power, the jet strongly interacting with a dense ISM, or a combination of these factors. The jet frustration paradigm is supported by high-resolution images that show distinct asymmetry in some CSS radio sources (Saikia et al. 1995; Saikia & Gupta 2003; Orienti et al. 2007).

The galaxies that host CSS sources are generally massive early-type galaxies with little star formation (SF), but a subset of the CSS population are known to exhibit enhanced SF (de Vries et al. 1998, 2000; Drake et al. 2004; Tadhunter et al. 2011; Dicken et al. 2012; O'Dea & Saikia 2021). A systematic study of SF in a large sample of CSS host galaxies may help shed light on why some CSS sources are star-forming and constrain the evolutionary path of these RLAGN. Such studies have previously been problematic as most samples of CSS sources consisted of objects with high radio luminosity that are rare in the local Universe. Consequently, the relatively shallow wide-field multiwavelength surveys that can readily provide star formation rates (SFRs) usually do not cover the high luminosity radio sources and expensive targeted observations are often necessary. The advent of deep, wide-field radio continuum surveys with high angular resolution is now making these types of systematic studies feasible (Sadler 2016).

The Faint Images of the Radio Sky at Twenty cm survey (FIRST; Becker et al. 1995) and the Very Large Array Sky Survey (VLASS; Lacy et al. 2020), which have angular resolutions of  $5.^{\prime\prime}4$  and  $3^{\prime\prime}$  respectively, are well suited to identifying compact radio sources brighter than  $\approx 1\,\mathrm{mJy}$ . Furthermore, these surveys observe at different frequencies; FIRST at  $1.4\,\mathrm{GHz}$  and VLASS at  $3\,\mathrm{GHz}$ . Using FIRST and VLASS data together is a pragmatic approach to measuring the spectral indices of large numbers of faint compact radio sources (Gordon et al. 2021). Both FIRST and VLASS cover the  $\approx 10,000\,\mathrm{deg}^2$  footprint of the Sloan Digital Sky Survey

(SDSS; York et al. 2000) which provides optical measurements and derived properties, including SFRs, for  $\sim \! 10^6$  galaxies. Combining FIRST, VLASS, and SDSS therefore has the potential to be an effective method for studying SF in a large number of CSS sources in the local Universe.

In this Letter we use data from FIRST, VLASS, and SDSS to investigate the relationship between radio source size and SF in CSS sources. The selection of CSS sources is described in Section 2. In Section 3 we compare the radio sizes and SFRs of our CSS sources. We discuss our results in Section 4 and state our conclusions in Section 5. Throughout this work we assume a flat  $\Lambda$ CDM cosmology with h=0.7,  $H_0=100\ h\ {\rm km\ s}^{-1}\ {\rm Mpc}^{-1}$ ,  $\Omega_m=0.3$ , and  $\Omega_\Lambda=0.7$ .

#### 2. Sample Selection

To identify likely CSS sources we start with the Best & Heckman (2012) catalog of radio galaxies in the SDSS Data Release 7 (DR7, Abazajian et al. 2009) spectroscopic sample. This catalog contains the host IDs of the radio sources, identifies sources where the radio emission is likely due to SF rather than an AGN, and where possible classifies RLAGN as either low- or high-excitation radio galaxies (LERGs or HERGs). As we are interested in compact radio AGN in this work, we select objects from the Best & Heckman (2012) catalog that are associated with a single detection in FIRST, excluding multi-FIRST-component sources from consideration.

High-frequency ( $\nu \sim 3$  GHz) information on our sources is obtained by crossmatching with the VLASS Epoch 1 component catalog (Gordon et al. 2021). We only search for VLASS components brighter than 3 mJy beam  $^{-1}$ , as fainter components have less reliable flux density measurements (See Section 3 of Gordon et al. 2021). A search radius of 5" is used which, given the on-sky component density of VLASS at S > 3 mJy ( $\sim 18$  deg  $^{-2}$ ), has an expected contamination level from false-positive matches of less than 0.05%. The 3 GHz flux density of our sources is then scaled by 1/0.87 to account for the systematic underestimation of flux density measurements in the VLASS catalog reported in Gordon et al. (2021). With flux densities at two different frequencies in hand, we determine the spectral index,  $\alpha$ , between 1.4 and 3 GHz for our sources.

The projected radio extents of CSS sources are smaller than 20 kpc (e.g., Fanti et al. 1985; O'Dea & Baum 1997; O'Dea & Saikia 2021). The VLASS catalog of Gordon et al. (2021) includes measurements of the source angular size after deconvolution from the beam.<sup>3</sup> Where the deconvolved angular size is nonzero, this is used to calculate the projected linear size (LS) of the source. If the source is so compact that it has a deconvolved angular size of zero in VLASS, then we use the uncertainty in the angular size to estimate an upper limit on the LS.

We select our likely CSS sources as having LS < 20 kpc and  $\alpha + \sigma_{\alpha} < -0.5$ , identifying 1109 objects. In Figure 1 we compare the redshifts and 1.4 GHz luminosities of this sample. By using only sources at z < 0.2 we select a volume-limited sample complete down radio luminosities of  $L_{1.4~\rm GHZ} > 10^{24}~\rm W~Hz^{-1}$ . This sample contains 259 CSS candidates, all but 38 (15%) of which are classified as LERGs. The radiatively efficient central engines in HERGs can impact the observed properties of the host galaxy, including spectral line

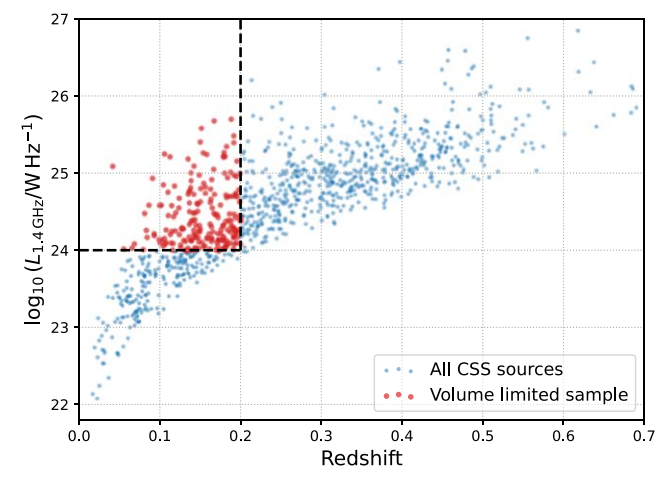


**Figure 1.** Redshift and 1.4 GHz luminosity distributions for our selection of CSS sources. Our volume-limited sample (red circles) is defined as having z < 0.2 and  $L_{1.4~\rm GHZ} > 10^{24}~\rm W~Hz^{-1}$ .

measurements used in determining SFRs. Conversely, the radiatively inefficient central engines of LERGs do not produce the high-energy photons necessary to bias spectral line measurements (Hardcastle et al. 2006). We therefore exclude the 38 sources not classified as LERGs. Finally,  $\approx\!20\%$  of single-FIRST-component RLAGN are expected to be multicomponent sources in VLASS (Gordon et al. 2019). To ensure we are only using sources with reliable sizes and spectral indices, we visually inspect the VLASS maps using SAOImage DS9 (Joye & Mandel 2003) with the catalog components overlaid. As a result we remove 55 multi-VLASS-component sources from our sample, leaving 166 CSS sources that we use for the analysis presented in this Letter.

# 3. Comparing Star Formation and Linear Size in CSS Sources

All of our CSS sources have host galaxies with spectral line measurements, stellar masses  $(M_*)$  and SFRs in the Max-Plank-Institut für Astrophysik/Johns Hopkins University (MPA/JHU) value added catalog for SDSS DR7<sup>4</sup> (Kauffmann et al. 2003; Brinchmann et al. 2004; Tremonti et al. 2004). In Figure 2 we plot the stellar masses and SFRs of our CSS sources. For reference we also show the distribution of all galaxies at z < 0.2 in SDSS DR7 as gray shaded contours. Galaxies in SDSS are split into two populations of "starforming" and "passive" at a specific star formation rate (sSFR = SFR/ $M_*$ ) of approximately 0.01 Gyr<sup>-1</sup> (shown by the black dashed line in Figure 2). The majority of our CSS sources are hosted by passive high-mass galaxies, with only 24 (14%) having  $sSFR > 0.01 \text{ Gyr}^{-1}$ . We confirm these have a similar redshift distribution to the passive CSS hosts in our sample by performing a Kolmogorov-Smirnov (KS) test, which returns a p-value of 0.75.

With SF being rare in CSS sources, one might ask whether there are differences between CSS sources with SF and CSS sources hosted by passive galaxies? One of the most fundamental properties of RLAGN is their size, i.e., how far the jets have traveled from the central engine. To assess if the sizes of CSS sources with SF and passive hosts differ, we plot the LS of our CSS sources versus their host sSFR in

These measurements are produced by the source-finder PyBDSF (Mohan & Rafferty 2015).

<sup>4</sup> https://wwwmpa.mpa-garching.mpg.de/SDSS/DR7/

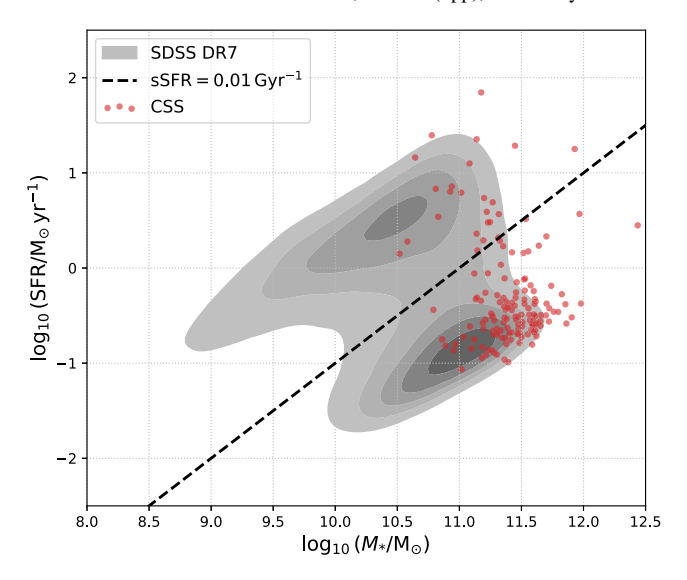


**Figure 2.** The stellar masses and star formation rates of our CSS sources (red circles). The gray shaded contours show the distributions for SDSS DR7. The black dashed line shows a fixed specific star formation rate of  $0.01 \, \text{Gyr}^{-1}$ .

Figure 3(a). CSS sources with sSFR < 0.01 Gyr<sup>-1</sup> are seen at all sizes in our sample (0 < LS < 20 kpc). However, higher sSFRs (sSFR > 0.01 Gyr<sup>-1</sup>) are only seen in CSS sources with LS  $\lesssim$  8 kpc. If we divide the CSS population at LS = 10 kpc, 17.9 $^{+3.8}_{-2.8}\%$  of sources with LS < 10 kpc have sSFR > 0.01 Gyr<sup>-1</sup>, compared to 0.0 $^{+0.5}_{-0.0}\%$  at LS  $\geqslant$  10 kpc. The uncertainties in these population fractions are estimated using the binomial approach outlined in Cameron (2011), and suggest a  $\approx$ 2.9 $\sigma$  excess of star-forming hosts in the smaller CSS sources.

The SFR measurements in SDSS are based on either the  ${\rm H}\alpha$  luminosity or the strength of the 4000 Å break,  $D_{4000}$ , depending on the spectral line properties of the galaxy (Brinchmann et al. 2004). In panels (b) and (c) of Figure 3 we show both of these observable properties complement our findings with respect to the derived sSFRs shown in Figure 3(a). Where  ${\rm H}\alpha$  is detected (signal-to-noise ratio  ${\rm [S/N]}>3$ ), the strongest  ${\rm H}\alpha$  emission lines are found nearly exclusively in CSS sources with LS < 6 kpc (Figure 3(b)). When considering  $D_{4000}$ , the weakest breaks —indicating young stellar populations—are found only in CSS sources with LS  $\lesssim$  10 kpc (Figure 3(c)).

A further test of the relative compactness of CSS sources with enhanced SF is to investigate how the infrared (IR) colors of the host change with LS. To this end we obtain IR information from the Wide-field Infrared Survey Explorer telescope (WISE; Wright et al. 2010) AllWISE catalog (Cutri et al. 2013, 2014). The WISE W2 (4.3  $\mu$ m) and W3 (12  $\mu$ m) filters can be used to identify star-forming galaxies. Additionally, the W1 (3.4  $\mu$ m) and W2 filters can identify galaxies where the IR colors are contaminated by AGN emission. From our sample of CSS sources, 102 (61%) are detected (S/N > 2) in the W1, W2, and W3 bands. Of these 102 galaxies, six have W1 - W2 > 0.5, indicating that their IR colors are dominated by the AGN (Mingo et al. 2016). For the remaining 96 CSS sources, we plot their W2-W3 color against LS in Figure 3(d). Adopting the criteria of Mingo et al. (2016), galaxies with

- 1. W2 W3 < 1.6 are passive,
- 2. 1.6 < W2 W3 < 3.4 are star-forming,

3. and W2 – W3 > 3.4 are (ultra)luminous infrared galaxies ([UlLIRGs).

Panel (d) of Figure 3 is consistent with panels (a)–(c), showing that nearly all CSS sources with IR colors indicative of SF have LS < 8 kpc. For CSS sources with LS < 10 kpc,  $40.0^{+5.5}_{-5.0}\%$  have star-forming WISE colors. On the other hand, only  $5.9^{+11.3}_{-1.9}\%$  of CSS sources with LS  $\geqslant$  10 kpc have WISE colors associated with star-forming galaxies—a deficit relative to the sub 10 kpc population at  $\approx$ 2.8 $\sigma$  confidence.

#### 4. Discussion

#### 4.1. Physical Interpretation

Our data show that where excess SF is present in CSS sources, those sources are limited to scales smaller than  $\approx 10$  kpc. At first glance, there are three likely possibilities that might explain this observation.

- 1. The jet itself has triggered a brief period of SF (e.g., Rees 1989; Labiano et al. 2008; Duggal et al. 2021).
- 2. A dense ISM is inhibiting the propagation of the radio jet resulting in its confinement to scales ≤10 kpc.
- The AGN is younger than the SF, limiting the time available for the radio jets to propagate away from the central engine.

To explore these scenarios, we compare the expected evolution of radio jets in these sources to the timescale on which the SF is detectable. In order to estimate the typical age of the jets in our CSS sources with enhanced SF, we simulate three "toy model" jets using the semianalytical radio jet evolution code of Hardcastle (2018). The median 1.4 GHz luminosity of our sample is  $10^{24.3}$  W Hz<sup>-1</sup>. For this simulation we assume a universal pressure profile (Arnaud et al. 2010) for galaxies in a halo of mass  $M_{500} = 10^{13.5} M_{\odot}$ . In this scenario, a radio source with LS = 10 kpc and  $L_{1.4 \text{ GHz}} = 10^{24.3}$  W Hz<sup>-1</sup> is expected to have a jet power, Q, of  $\sim 10^{36}$  W (see Figure 4(a)). Such a jet will have taken  $\approx 8$  Myr to reach its current size, and would reach a linear size of  $\approx 19$  kpc within 20 Myr of being switched on (see Figure 4(b)).

The increase in radio luminosity shown for our toy model jets as the radio source grows is consistent with our data. In Figure 5(a) we show the distributions of  $L_{1.4\,\mathrm{GHz}}$  for small (LS < 10 kpc) and larger (LS  $\geqslant$  10 kpc) CSS sources in our sample. Performing a KS test returns a p-value of  $8\times10^{-3}$ , showing these distributions to be statistically different. The smaller CSS sources have a median radio luminosity of  $10^{24.26}\,\mathrm{W\,Hz^{-1}}$ , while the larger sources have a median value of  $10^{24.49}\,\mathrm{W\,Hz^{-1}}$ . Such a change in luminosity for a  $10^{36}\,\mathrm{W}$  jet would be expected as it grows from a linear size of  $\approx$ 6 kpc to  $\approx$ 12 kpc (see Figure 4(a)). The  $L_{1.4\,\mathrm{GHz}}$  distribution of the CSS sources with sSFR > 0.01 Gyr $^{-1}$  (Figure 5(b)) is consistent with the luminosity distribution of the smaller CSS sources, having a KS derived p-value of 0.26.

The SF indicators shown in Figure 3 are visible for different time periods after SF ends. H $\alpha$  emission is the result of ionization of the ISM by massive O-type stars, limiting its visibility to  $\approx$ 20 Myr after the cessation of SF (Kennicutt 1998). Conversely,  $D_{4000}$  is affected by the entire stellar population and evolves slowly following a starburst, taking several hundred Myr for a strong break to develop (Goto et al. 2008). IR colors resulting from SF evolve on a timescale between the two extremes of H $\alpha$  and  $D_{4000}$ . The WISE W3

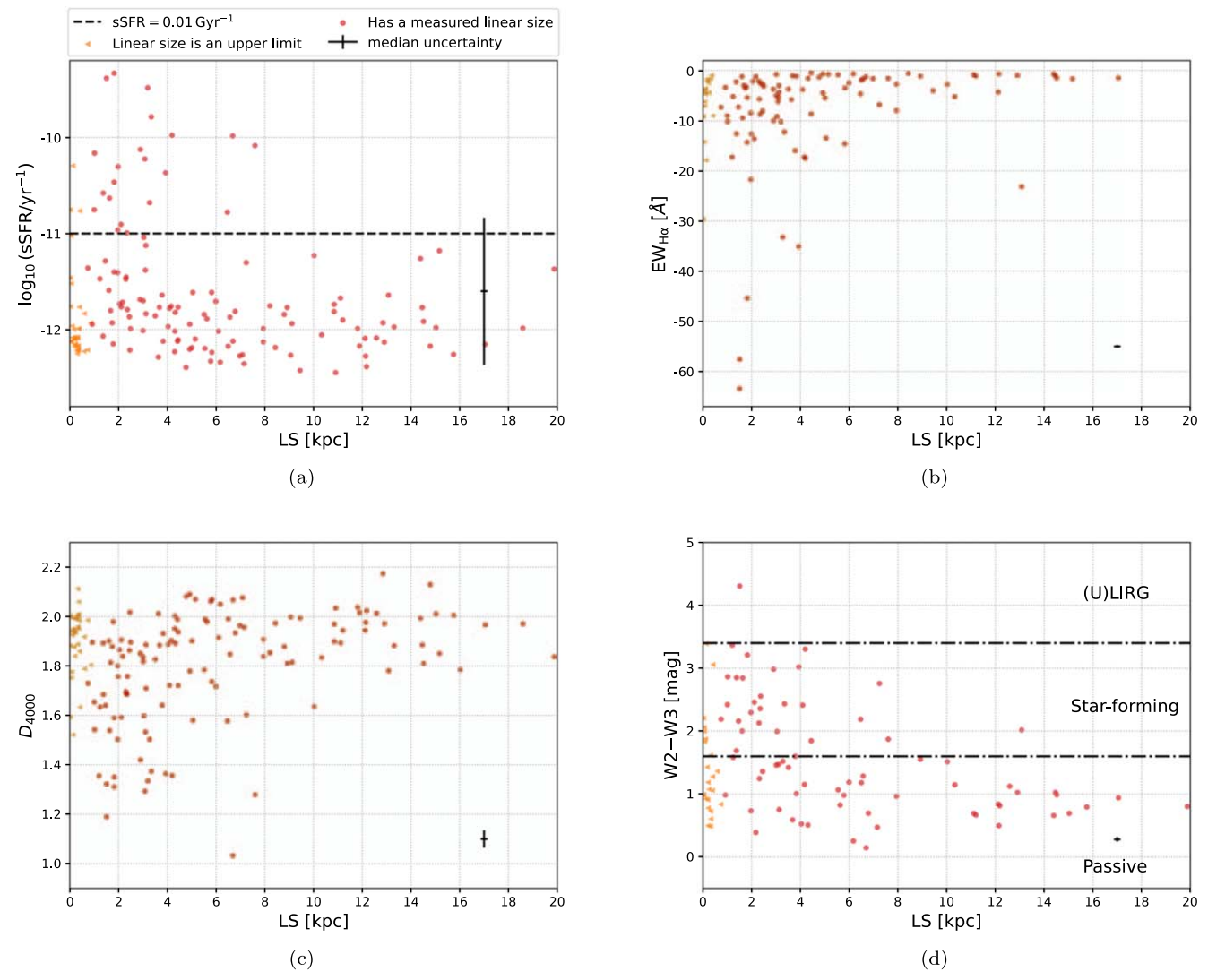


Figure 3. Comparisons of star-forming indicators and linear size (LS) for our CSS sources. Panel (a) shows the SDSS sSFR measurements for our CSS sources with a black dashed line indicating sSFR =  $0.01 \, \text{Gyr}^{-1}$ . Panel (b) shows the equivalent width of  $H\alpha$  (EW $_{H\alpha}$ ) for our CSS sources where this line is detected at S/N > 3, while panel (c) shows the strength of the 4000 Å break. In Panel (d) the WISE colors are shown for galaxies where the AGN does not dominate the IR color (W1 - W2 < 0.5). Here the dotted-dashed lines separate colors associated with passive galaxies, star-forming galaxies, and (U)LIRGs. In all panels orange triangles denote CSS sources where the LS is an upper limit, and the black cross shows the median uncertainty for the data points.

band traces SF through the polycyclic aromatic hydrocarbons associated with B-type stars that live for  $\approx 100$  Myr following a starburst (Peeters et al. 2004; Jarrett et al. 2011).

Assuming a jet age on the order of  $\sim \! 10 \, \mathrm{Myr}$ , the absence of low  $D_{4000}$  values in CSS sources with LS  $\gtrsim 10 \, \mathrm{kpc}$  suggests that the bulk of SF ceased hundreds of Myr prior to the jet being triggered. Our results are thus inconsistent with the AGN jet triggering the SF unless jet propagation is frustrated for hundreds of Myr. On the other hand, the presence of strong H $\alpha$  emission in CSS sources with LS  $\lesssim 10 \, \mathrm{kpc}$  is indicative of active SF as recently as 10 Myr prior to the jet being triggered. Future observations that measure the jet (a)symmetry and hotspot proper motions are necessary to test if these sources are indeed frustrated.

A tantalizing explanation for our results is that of galaxy mergers—a known trigger for both SF and AGN (e.g., Ellison et al. 2013; Pearson et al. 2019; Gao et al. 2020; Pierce et al. 2022, 2023). In galaxy mergers SF is episodic and the time required for gas to fall into the central engine means that RLAGN are not expected to be triggered until a

few hundred Myr after the first starburst (Tadhunter et al. 2005; Peirani et al. 2010; Shabala et al. 2017). A final starburst in the merger sequence that ceases  $\approx 10$  Myr prior to the jet being triggered, and has a much smaller burst fraction than the initial starburst several hundred Myr earlier, might produce the observed H $\alpha$  with a limited impact on  $D_{4000}$ . It is therefore prudent to ask if our sample of CSS sources with enhanced SF are associated with mergers? To this end we visually inspect optical images obtained from the ninth data release of the Dark Energy Spectroscopic Instrument Legacy Imaging Surveys (Dey et al. 2019) for the 24 CSS sources with sSFR  $> 0.01 \,\text{Gyr}^{-1}$ . We find that 11 (46%) show clear evidence of tidal features indicative of a recent major galaxy-galaxy interaction. This is a higher incidence than the 28% of the LERG population shown to have tidal features in Gordon et al. (2019). The relatively high fraction of our sample with tidal features suggests that mergers likely explain at least some CSS sources with enhanced SF, and this warrants further study.

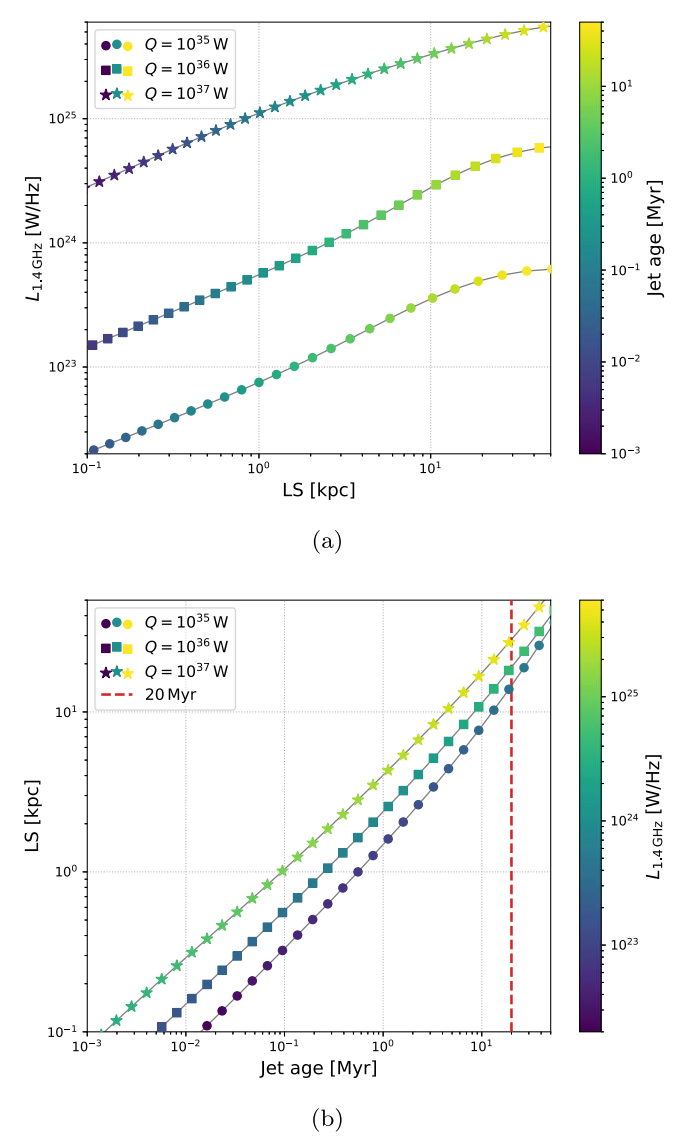
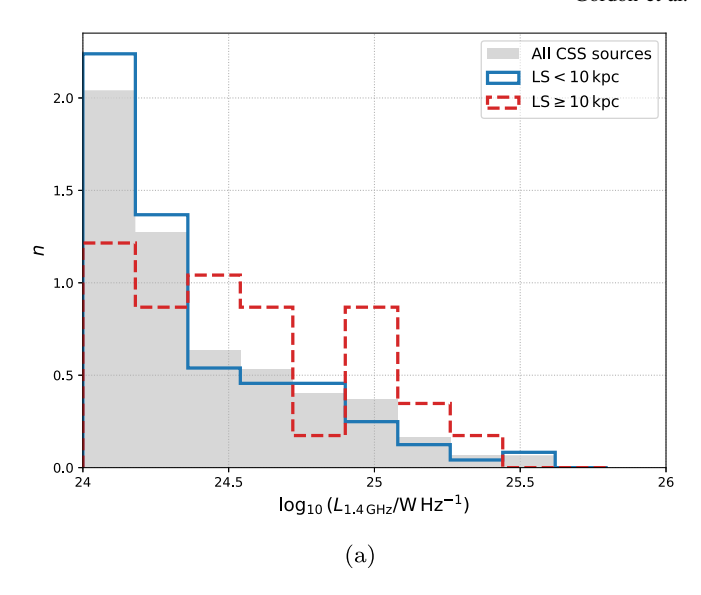


**Figure 4.** Three toy model jets simulated using the semianalytical code of Hardcastle (2018) with powers  $Q = 10^{35}$  W (circles),  $Q = 10^{36}$  W (squares), and  $Q = 10^{37}$  W (stars). Panel (a) shows the evolution of 1.4 GHz luminosity with linear size colored by the jet age. Panel (b) shows the linear size growth as a function jet age, with the points colored by  $L_{1.4 \text{ GHz}}$ . The red dashed line in panel (b) shows the 20 Myr typical lifetime of O-type stars.

# 4.2. Are Our CSS Sources Really Variable Sources?

We have selected our CSS sources using legacy data from two different radio surveys. Because these observations were not made simultaneously—two decades separate FIRST and VLASS—it is possible the difference in flux density measurements may be an effect of radio source variability rather than the shape of spectral energy distribution. Variable radio sources typically have very compact morphologies. Nyland et al. (2020) show that sources showing variability between FIRST and VLASS have LS < 1 kpc, while Wołowska et al. (2021) use VLBI imaging to show such sources typically have sizes of just a few tens of parsecs.

Of the 24 CSS sources with sSFR  $> 0.01 \, \mathrm{Gyr}^{-1}$ , only three are completely unresolved by VLASS (shown as upper limits in Figure 3). A further 9 of these 24 sources have measured linear sizes below 2 kpc, notably all of which are greater than 1 kpc. The other half of our CSS sample with enhanced SF have



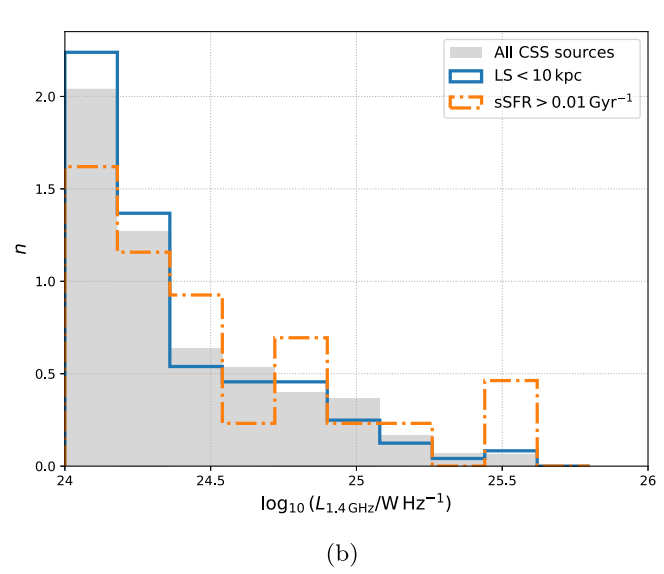


**Figure 5.** Normalized distributions of  $L_{1.4~\mathrm{GHz}}$  for subsamples of our CSS sources. Both panels show the full CSS sample as a solid gray histogram, and the CSS sources with LS < 10 kpc as blue solid line. Panel (a) shows a comparison with sources having LS  $\geqslant$  10 kpc (red dashed line), while Panel (b) shows the radio luminosities of CSS sources with sSFR > 0.01 Gyr<sup>-1</sup> (orange dotted–dashed line).

 $2\,\mathrm{kpc} < LS < 8\,\mathrm{kpc}$  and are therefore larger than variable sources are expected to be. If we were to cautiously assume that the 12 sources within our sample with enhanced SF and LS < 2 kpc are all variable sources, then our conclusion would still be valid: CSS sources with enhanced SF are smaller than  $\approx \! 10\,\mathrm{kpc}$ .

## 5. Conclusions

In this Letter we have systematically investigated the relationship between star formation and radio source size in CSS sources. We find that where enhanced SF is present the radio source has LS  $\lesssim 10\,$  kpc, while passive hosts are seen in CSS sources with  $0\leqslant LS<20\,$  kpc. Based on simulated jet propagation times, the absence of CSS hosts with weak 4000 Å break strengths at LS  $\gtrsim 10\,$  kpc suggests the bulk of SF ceased several hundred Myr before the AGN jet was triggered. The presence of  $H\alpha$  emission in CSS sources with LS  $< 10\,$  kpc indicates that some SF occurred  $\approx \! 10\,$  Myr prior to the jet

triggering. We interpret this apparent ambiguity as being the result of episodic SF in these CSS sources where the later starbursts have a lower "burst fraction," potentially resulting from galaxy–galaxy interactions.

We thank the anonymous referee for their helpful report that has improved the quality of this work. Y.A.G. is supported by U.S. National Science Foundation grant AST 20-09441. C.P. O., S.A.B., and C.D. are supported by NSERC, the National Sciences and Engineering Research Council of Canada.

The VLA is operated by The National Radio Astronomy Observatory, a facility of the National Science Foundation operated under cooperative agreement by Associated Universities, Inc.

Funding for the SDSS and SDSS-II has been provided by the Alfred P. Sloan Foundation, the Participating Institutions, the National Science Foundation, the U.S. Department of Energy, the National Aeronautics and Space Administration, the Japanese Monbukagakusho, the Max Planck Society, and the Higher Education Funding Council for England. The SDSS website is <a href="http://www.sdss.org/">http://www.sdss.org/</a>.

The SDSS is managed by the Astrophysical Research Consortium for the Participating Institutions. The Participating Institutions are the American Museum of Natural History, Astrophysical Institute Potsdam, University of Basel, University of Cambridge, Case Western Reserve University, University of Chicago, Drexel University, Fermilab, the Institute for Advanced Study, the Japan Participation Group, Johns Hopkins University, the Joint Institute for Nuclear Astrophysics, the Kavli Institute for Particle Astrophysics and Cosmology, the Korean Scientist Group, the Chinese Academy of Sciences (LAMOST), Los Alamos National Laboratory, the Max-Planck-Institute for Astronomy (MPIA), the Max-Planck-Institute for Astrophysics (MPA), New Mexico State University, Ohio State University, University of Pittsburgh, University of Portsmouth, Princeton University, the United States Naval Observatory, and the University of Washington.

WISE is a joint project of the University of California, Los Angeles, and the Jet Propulsion Laboratory/California Institute of Technology, and NEOWISE, which is a project of the Jet Propulsion Laboratory/California Institute of Technology. WISE and NEOWISE are funded by the National Aeronautics and Space Administration.

Facilities: VLA, Sloan, WISE.

Software: Astropy (Astropy Collaboration et al. 2013, 2018, 2022), Matplotlib (Hunter 2007), NumPy (Harris et al. 2020), SAOImage DS9 (Joye & Mandel 2003), SciPy (Virtanen et al. 2020), Seaborn (Waskom 2021), TOPCAT (Taylor 2005).

#### ORCID iDs

Yjan A. Gordon https://orcid.org/0000-0003-1432-253X Christopher P. O'Dea https://orcid.org/0000-0001-6421-054X

Stefi A. Baum https://orcid.org/0000-0002-4735-8224 Keith Bechtol https://orcid.org/0000-0001-8156-0429 Chetna Duggal https://orcid.org/0000-0001-7781-246X Peter S. Ferguson https://orcid.org/0000-0001-6957-1627

#### References

Abazajian, K. N., Adelman-McCarthy, J. K., Agüeros, M. A., et al. 2009,
 ApJS, 182, 543
 An, T., & Baan, W. A. 2012, ApJ, 760, 77

```
An, T., Wu, F., Yang, J., et al. 2012, ApJS, 198, 5
Arnaud, M., Pratt, G. W., Piffaretti, R., et al. 2010, A&A, 517, A92
Astropy Collaboration, Price-Whelan, A. M., Lim, B. M., et al. 2022, ApJ,
Astropy Collaboration, Price-Whelan, A. M., Sipőcz, B. M., et al. 2018, AJ,
   156, 123
Astropy Collaboration, Robitaille, T. P., Tollerud, E. J., et al. 2013, A&A,
Becker, R. H., White, R. L., & Helfand, D. J. 1995, ApJ, 450, 559
Best, P. N., & Heckman, T. M. 2012, MNRAS, 421, 1569
Blandford, R., Meier, D., & Readhead, A. 2019, ARA&A, 57, 467
Brinchmann, J., Charlot, S., White, S. D. M., et al. 2004, MNRAS, 351, 1151
Cameron, E. 2011, PASA, 28, 128
Cutri, R. M., Wright, E. L., Conrow, T., et al. 2014, VizieR On-line Data
   Catalog: J/MNRAS/484/1021
Cutri, R. M., Wright, E. L., Conrow, T., et al. 2013, in Explanatory Supplement
   to the AllWISE Data Release Products, Explanatory Supplement to the
   AllWISE Data Release Products, ed. R. M. Cutri et al.
Dabhade, P., Gaikwad, M., Bagchi, J., et al. 2017, MNRAS, 469, 2886
Dallacasa, D., Fanti, C., Fanti, R., Schilizzi, R. T., & Spencer, R. E. 1995,
   A&A, 295, 27
de Vries, W. H., O'Dea, C. P., Barthel, P. D., et al. 2000, AJ, 120, 2300
de Vries, W. H., O'Dea, C. P., Baum, S. A., et al. 1998, ApJ, 503, 156
Dey, A., Schlegel, D. J., Lang, D., et al. 2019, AJ, 157, 168
Dicken, D., Tadhunter, C., Axon, D., et al. 2012, ApJ, 745, 172
Drake, C. L., McGregor, P. J., & Dopita, M. A. 2004, AJ, 128, 955 Duggal, C., O'Dea, C., Baum, S., et al. 2021, AN, 342, 1087
Ellison, S. L., Mendel, J. T., Patton, D. R., & Scudder, J. M. 2013, MNRAS,
Fanaroff, B. L., & Riley, J. M. 1974, MNRAS, 167, 31P
Fanti, C., Fanti, R., Dallacasa, D., et al. 1995, A&A, 302, 317
Fanti, C., Fanti, R., Parma, P., Schilizzi, R. T., & van Breugel, W. J. M. 1985,
   A&A, 143, 292
Fanti, R., Fanti, C., Schilizzi, R. T., et al. 1990, A&A, 231, 333
Gao, F., Wang, L., Pearson, W. J., et al. 2020, A&A, 637, A94
Gordon, Y. A., Boyce, M. M., O'Dea, C. P., et al. 2021, ApJS, 255, 30
Gordon, Y. A., Pimbblet, K. A., Kaviraj, S., et al. 2019, ApJ, 878, 88
Goto, T., Yagi, M., & Yamauchi, C. 2008, MNRAS, 391, 700
Hardcastle, M. J. 2018, MNRAS, 475, 2768
Hardcastle, M. J., Evans, D. A., & Croston, J. H. 2006, MNRAS, 370,
Harris, C. R., Millman, K. J., van der Walt, S. J., et al. 2020, Natur, 585, 357
Hunter, J. D. 2007, CSE, 9, 90
Ishwara-Chandra, C. H., & Saikia, D. J. 1999, MNRAS, 309, 100
Jarrett, T. H., Cohen, M., Masci, F., et al. 2011, ApJ, 735, 112
Joye, W. A., & Mandel, E. 2003, in ASP Conf. Ser. 295, Astronomical Data
   Analysis Software and Systems XII, ed. H. E. Payne, R. I. Jedrzejewski, &
   R. N. Hook (San Francisco, CA: ASP), 489
Kauffmann, G., Heckman, T. M., White, S. D. M., et al. 2003, MNRAS,
   341.33
Kennicutt, R. C. J. 1998, ARA&A, 36, 189
Labiano, A., O'Dea, C. P., Barthel, P. D., de Vries, W. H., & Baum, S. A.
   2008, A&A, 477, 491
Lacy, M., Baum, S. A., Chandler, C. J., et al. 2020, PASP, 132, 035001
Mingo, B., Watson, M. G., Rosen, S. R., et al. 2016, MNRAS, 462, 2631
Mohan, N., & Rafferty, D. 2015, PyBDSF: Python Blob Detection and Source
  Finder, Astrophysics Source Code Library, record ascl:1502.007
Nyland, K., Dong, D. Z., Patil, P., et al. 2020, ApJ, 905, 74
O'Dea, C. P. 1998, PASP, 110, 493
O'Dea, C. P., & Baum, S. A. 1997, AJ, 113, 148
O'Dea, C. P., Baum, S. A., & Stanghellini, C. 1991, ApJ, 380, 66
O'Dea, C. P., & Saikia, D. J. 2021, A&ARv, 29, 3
Orienti, M., Dallacasa, D., & Stanghellini, C. 2007, A&A, 461, 923
Owsianik, I., & Conway, J. E. 1998, A&A, 337, 69
Padovani, P. 2017, NatAs, 1, 0194
Pearson, W. J., Wang, L., Alpaslan, M., et al. 2019, A&A, 631, A51
Peeters, E., Spoon, H. W. W., & Tielens, A. G. G. M. 2004, ApJ, 613, 986
Peirani, S., Crockett, R. M., Geen, S., et al. 2010, MNRAS, 405, 2327
Pierce, J. C. S., Tadhunter, C., Almeida, C. R., et al. 2023, MNRAS, Advance
  Acces
Pierce, J. C. S., Tadhunter, C. N., Gordon, Y., et al. 2022, MNRAS, 510, 1163
Polatidis, A. G., & Conway, J. E. 2003, PASA, 20, 69
Rees, M. J. 1989, MNRAS, 239, 1P
Sadler, E. M. 2016, AN, 337, 105
Saikia, D. J., & Gupta, N. 2003, A&A, 405, 499
Saikia, D. J., Jeyakumar, S., Wiita, P. J., Sanghera, H. S., & Spencer, R. E.
   1995, MNRAS, 276, 1215
```

```
Salpeter, E. E. 1964, ApJ, 140, 796
Shabala, S. S., Deller, A., Kaviraj, S., et al. 2017, MNRAS, 464, 4706
Spencer, R. E., Schilizzi, R. T., Fanti, C., et al. 1991, MNRAS, 250, 225
Tadhunter, C., Holt, J., González Delgado, R., et al. 2011, MNRAS, 412, 960
Tadhunter, C., Robinson, T. G., González Delgado, R. M., Wills, K., & Morganti, R. 2005, MNRAS, 356, 480
Taylor, M. B. 2005, in ASP Conf. Ser. 347, Astronomical Data Analysis
```

Taylor, M. B. 2005, in ASP Conf. Ser. 347, Astronomical Data Analysis Software and Systems XIV, ed. P. Shopbell, M. Britton, & R. Ebert (San Francisco, CA: ASP), 29

Tremonti, C. A., Heckman, T. M., Kauffmann, G., et al. 2004, ApJ, 613, 898

```
van Breugel, W., Miley, G., & Heckman, T. 1984, AJ, 89, 5
Virtanen, P., Gommers, R., Oliphant, T. E., et al. 2020, NatMe, 17, 261
Waskom, M. L. 2021, JOSS, 6, 3021
Wilkinson, P. N., Booth, R. S., Cornwell, T. J., & Clark, R. R. 1984, Natur,
```

308, 619

Willis, A. G., Strom, R. G., & Wilson, A. S. 1974, Natur, 250, 625
Wołowska, A., Kunert-Bajraszewska, M., Mooley, K. P., et al. 2021, ApJ, 914, 22

Wright, E. L., Eisenhardt, P. R. M., Mainzer, A. K., et al. 2010, AJ, 140, 1868 York, D. G., Adelman, J., Anderson, J. E. J., et al. 2000, AJ, 120, 1579